Eur. Phys. J. Plus (2019) **134**: 39
DOI 10.1140/epjp/i2019-12427-3

THE EUROPEAN PHYSICAL JOURNAL PLUS

Regular Article

Sodium dodecyl sulfate microaggregates with diversely developed surfaces: Formation from free microdroplets of colloidal suspension

Justice Archer[1,a], Maciej Kolwas[1,b], Mariusz Woźniak[1], Daniel Jakubczyk[1], Krystyna Kolwas[1], Gennadiy Derkachov[1], and Tomasz Wojciechowski[2]

[1] Institute of Physics, Polish Academy of Sciences, al. Lotników 32/46, PL-02668 Warsaw, Poland
[2] International Research Centre MagTop, Institute of Physics, Polish Academy of Sciences, al. Lotników 32/46, PL-02668 Warsaw, Poland

Received: 27 July 2018
Published online: 28 January 2019

Abstract. Unsupported drying of microdroplets of colloidal suspension can lead to the formation of complex micro-morphologies with quasi-spherical symmetry. Herein, drying of levitating microdroplets of suspension of SiO_2 nanospheres in diethylene glycol (DEG) with sodium dodecyl sulfate (SDS) is reported as a method for producing such microstructures with diversely developed surfaces. Dried products are "soft-landed" on a substrate and studied with scanning electron microscopy (SEM). The smallest SDS/SiO_2 composites with the surface formed of crystallised SDS and interior filled with SiO_2 nanospheres preserve the spherical symmetry. Larger microdroplets with higher initial mass fractions of SDS dry up to developed microstructures with SiO_2 nanospheres arranged in-between the crystallised SDS flakes which are similar to curved lobe cabbage leaves or "desert rose"-like structures with radially directed SDS crystals. Largest microdroplets with highest initial mass fractions of SDS formed doughnut-shaped micro-containers filled with aggregated SiO_2 nanospheres. In all these, SiO_2 nanospheres served as a frame for the SDS crystallisation.

1 Introduction

Evaporation-driven assembly of nanoparticles in a drying microdroplet is an ideal mechanism for building micro- and nanostructured materials with tailor made properties at scales where direct structural manipulation is impossible. Over the years, a number of bottom-up methods [1–10] have been reported for obtaining the final dry products by drying of microdroplets with a variety of solid inclusions. These methods have been categorised by [11] into two as the wet-self assembly (WSA) and the dry-self assembly (DSA) methods. The WSA approaches are usually based on using emulsions. The spherical aggregates are formed by the arrangement of the suspended particles inside the droplets emulsified in the liquid [12]. Well-known drawbacks associated with the WSA methods are mainly due to the necessity of demulsification processes allowing extraction of the final dry micro- or nano-products and the difficulty in controlling the shape of the final products. The fabrication of solid capsules known as the colloidosomes [8], highly monodispersed spherical crystalline colloidal arrays (CCAs) [4] and of low-dimensional super-particles complex rattle-like structures and 2D plates [13] are typical examples based on the WSA method.

Techniques employing DSA methods are often considered to be more favourable in comparison to the WSA methods [1, 11, 12]. The DSA methods are mostly based on approaches where droplets of colloidal suspensions are dried in spray dryers [3, 9, 14], on solid surfaces [1, 5, 7] or in Leidenfrost levitation [6]. The most often used method is the spray drying technique [14, 15]. Creating complex micro- and nano-structured morphologies of nanosphere assemblies using spray drying is very appealing, but the process is sufficiently difficult and materially consuming from first principle [15–17]. Methods based on drying microdroplets of colloids on substrates are characterized by a strong impact of the wettability and treatment of the substrate surface on the final structure formation [10]. Similarly, the use of the

[a] *Present address*: Bristol Aerosol Research Centre, School of Chemistry, University of Bristol, Bristol, BS8 1TS, UK.
[b] e-mail: kolwas@ifpan.edu.pl

Leidenfrost effects has its own demerits. The method depends not only on the solvent nature but also on the substrate properties. Moreover, the bulk thermal conductivity of the substrate should guarantee sufficient transfer of energy from the substrate to the droplet [6,18].

Recently, we reported a versatile DSA method [19,20] of formation of highly ordered spherical aggregates from drying microdroplets of colloidal SiO_2 suspension by the evaporation of single microdroplets levitated in the linear electrodynamic quadrupole trap [21–23]. The use of electrodynamic trapping of microdroplets of colloidal suspensions provide a contactless versatile solution. It allows unsupported drying of the solvent/dispersion media [24,25], control and retention of the droplets/aggregates [26] as well as singly deposition ("soft-landing") of the final products with well-defined symmetries [19,20]. The technique requires less material implementation from first principles and does not require any pre-treatment of the substrates on which the dried particles are deposited.

It is known that the morphology and properties of the final micro- and or nano-structured dry products assembled via evaporation-driven processes can equally be modified by several mechanisms. These may include: chemical transformations [27], charge tuning [3], number concentration of the particles inside the initial droplet [5,28], choice of the solvent and nanoparticle sizes [7,29] as well as the addition of surfactant to the initial droplet composition [1,30]. The latter is known to have an effect on the interfacial tension and thereby on the shape of the droplet [31,32].

The anionic surfactant, sodium dodecyl sulfate (SDS) is perhaps one of the most widely studied surfactant with unique physical properties [33–36] that has found many applications in science and technology. The role of SDS in evaporation-driven assembly of nanoparticles have been widely explored [6,29,37–42]. For example, [37] used SDS as a capping agent to synthesise rose-like BiOBr nanostructures with exposed {111} facets via a facile solvothermal route. SDS has also been used with inorganic SiO_2 as a soft matrix component to produce hollow nano-composite capsules through evaporation-induced self-assembly by spray drying technique [29]. Reference [38] also used different molar ratios of SDS as a structure-directing agent for ZnO nanostructure synthesis by hydrothermal method at an elevated temperature. In their work, they observed that, increasing the amount of SDS to the mother liquor with constant amount of cetyltrimethylammonium bromide (CTAB) resulted in different morphologies of the ZnO nanostructures, from rods-spherical outlines and branched rod-like shapes to close-ranked structures of nanoparticles. Similarly, through hydrothermal route, [40] successfully synthesized 3D flower-like ZnO architectures assembled with numerous nanosheets with the aid of SDS. It has also been demonstrated that SDS is a highly effective structure-directing agent for producing box-like structures [41] and is observed elsewhere to cause complete suppression of the buckling phenomenon above an optimal value of 1% by weight [42]. Additionally, Blanch *et al.* [39] found out that attractive depletion in SDS was preferential for carbon nanotubes of larger diameter at higher concentrations of SDS.

To date, much less is known about the formation of complex microobjects with distinctively different, but controlled initial droplet parameters per-drop basis. Similarly, methods allowing purposive microobject morphology transformations by different concentrations (or mass fractions) of SDS in drying microdroplets, unperturbed by the presence of substrates, walls or chemicals are yet to be explored. Herein, we present a study based on electrodynamic levitation technique for drying composite microdroplets of colloidal suspensions and "soft-landing" of the dried microobjects for off-line scanning electron microscopy (SEM) imaging to explore drying of complex, multi-component mixtures of micro- and nano-droplets on a per-drop basis. The droplet is suspended in the linear electrodynamic quadrupole trap (LEQT), allowing unsupported solvent drying processes and microobject morphology evolution. The quasi-spherical symmetry is imposed on the drying microobject by the surface tension forces, which constitutes the uniqueness of the method. The single dry microobjects are deposited on a silicon substrate after solvent/dispersion medium evaporation and further analysed off-line with a SEM. Different microobjects of distinct shapes and sizes were obtained by tuning the initial parameters (size and the concentration of SDS) of the composite microdroplets in the mixture of DEG/SDS/SiO_2/H_2O colloidal suspension.

2 Experimental section

2.1 Materials and sample preparation

Diethylene glycol (DEG, BioUltra, purity $\geq$ 99.0% (GC)) and sodium dodecylsulfate, (SDS, ACS reagent grade, purity $\geq$ 99.0%) were both purchased from Sigma-Aldrich. DEG is a widely used solvent and is well-known for its efficient stabilisation of nanoparticles [43] and hence was chosen as a suitable solvent/dispersion medium for our sample preparation. Additionally, since DEG evaporates much slower than, *e.g.*, water at room temperature, it was chosen as a dispersion medium to model slow drying of the droplets under stabilised atmospheric conditions. Thus, it provides enough drying time for the arrangement of the suspended inclusions in the droplet during the drying process. Colloidal silica (SiO_2) nanospheres (C-SiO_2, 125 nm radius, initial mass and volume concentrations equal to 5% and 2.6%, respectively) was purchased from Corpuscular Inc. The silica nanospheres were non-functionalised and were considered to be negatively charged at the surface. However, the exact amount of charge of the individual silica nanospheres were not measured. Different molar concentrations (C) of DEG/SDS solutions (C = 20 mM, 40 mM, 70 mM and 100 mM) were prepared by dissolving weighed SDS in a measured volume of DEG. The solution was then sonicated for about

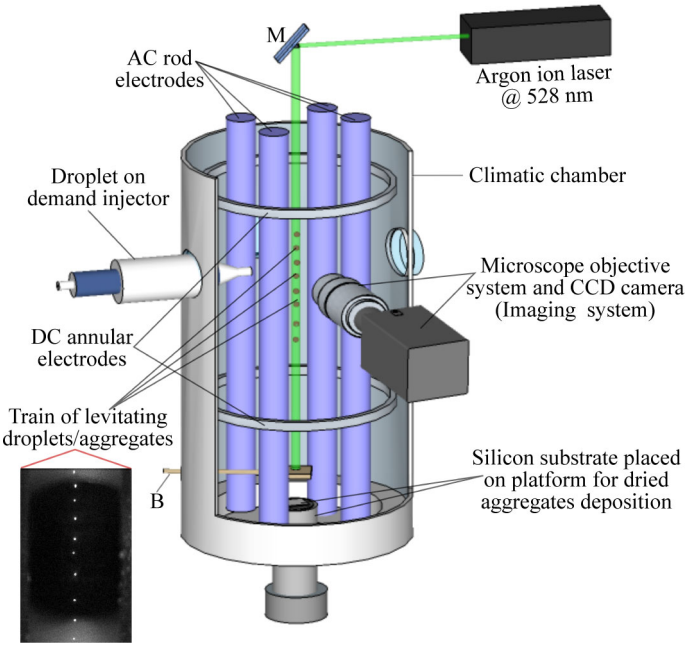

Fig. 1. Experimental setup with the linear electrodynamic quadrupole trap (LEQT). M — mounted mirror for directing laser beam into the trap; B — Blocker (for preventing stray droplets from contaminating the substrate surface); inset — photo of a train of levitating droplets/aggregates with similar charge polarity naturally spaced equally along the vertical axis of the LEQT as observed in the experiment by the imaging system.

15 minutes to ensure uniform mixing and passed through a syringe filter of pore size 0.22 μm (Chemland, Nylon 66 SFNY025022N) to remove any unwanted residual solid impurities. A colloidal SiO_2 (12.8 mg of SiO_2 nanospheres in 0.25 ml of the colloidal SiO_2/H_2O suspension) was then added to the filtered DEG/SDS solution to form the DEG/SDS/SiO_2/H_2O colloidal suspension. The final suspension was again sonicated to obtain uniform mixing and carefully transferred into the droplet-on-demand injector under controlled dust free environment to prevent contamination of the samples. The initial mass fractions of the DEG/SiO_2/H_2O components in the DEG/SDS/H_2O/SiO_2 mixture was kept nearly constant for the variable SDS concentrations. All the samples were prepared in insulin syringes. The initial solution/suspension concentration of the droplets injected into the trap were assumed equal to the prepared solution concentration [20].

2.2 Experimental setup and procedure

The experimental process involved three main stages: droplet generation, droplet evaporation/drying and single aggregate (microobject) deposition ("soft landing"). The droplet evaporation/drying process took place at the centre (vertical axis) of the LEQT. The trap consisted of four (4) spaced rod electrodes in a square pattern in vertical alignment with two spaced annular electrodes around them. A schematic of the experimental setup is shown in fig. 1. The rod electrodes, driven with an AC voltage ~ 10 kV, provided a time-varying quadrupole field that was used to constrain droplets to a point in the two-dimensional plane perpendicular to the rod axes, producing a line of stability along the geometric centre. A stabilising loop DC voltage (up to ± 1.1 kV) driven by a PID-type software controller was applied across the two annular electrodes to balance the weight of the constrained droplets. The DC voltage could also be regulated manually to control the vertical position of the droplet(s)/aggregate(s) along the line of stability in the trap. The LEQT was contained in a small climatic chamber made of double-walled air tight chamber that could be cooled/heated with Peltier elements. Hence, the temperature and atmospheric parameters (*e.g.*, humidity) in the trap were controlled. An average temperature of 296.2 ± 0.1 K and relative humidity of $30 \pm 3.5\%$ was maintained for all the droplet drying processes. The chamber was equipped with four side ports together with a top and bottom ports. The top and bottom ports served respectively for the laser light illumination of trapped droplets/aggregates along the line of stability and for insertion of the aggregate deposition platform.

Generation of charged microdroplets with well repeatable charge polarity on a per-drop basis into the trap was achieved with the droplet-on-demand injector [44] placed at one of the side ports of the LEQT. The sign of the charge on each droplet injected into the trap was pre-controlled by a pair of charging ring electrodes (charger). The rings were attached just in front of and just behind the ejection aperture of the nozzle. The approximate net charge ($\sim 6 \times 10^5$

elementary charges) deposited on the droplet was very similar from injection to injection (*i.e.*, same injection and trapping parameters). However, its value was controllable only to a limited extend due to the presence of strong fields around the trap electrodes. The droplet charge was considered constant since no droplet electrostatic fission (Coulomb explosions) [45, 46] were observed for all the droplet compositions we studied. The approximate initial droplet size was controlled with the parameters of the droplet-on-demand injector (nozzle diameter, driving pulse width, shape and amplitude) [47]. However, we noticed that the initial diameters of microdroplets from the DEG/SDS solution for the same injection parameters and same nozzles were larger in comparison to the droplets generated from the DEG/H_2O/SiO_2 colloidal suspensions. This effect was particularly visible for higher initial SDS concentrations and should be well expected due to the reduction of the surface tension caused by the SDS.

Droplets injected into the trap were illuminated by a control laser beam directed by the mirror M, along the vertical axis of the LEQT and were observed by the CCD camera placed at one of the side viewing ports. The live-view images provided by the CCD camera were used for the droplet position finding via the PID-type software controller. This enabled the droplet(s)/aggregate(s) positions to be stabilised along the vertical axis of the trap with the aid of the DC voltage applied to the annular electrodes.

The dry aggregates/microobject deposition process was realised by slowly lowering the DC field balancing their weight at the desired moment in time. Typically, the solution/suspension microdroplets were dried for 45 minutes to achieve fully dried stable and compact microproducts. The dry products were gently and singly deposited ("soft-landed") onto the silicon substrate placed on the deposition platform and further analysed off-line with SEM. The dimensions of the microobjects were found directly from SEM with a dedicated software (SmartTiff, Carl Zeiss SMT Ltd.).

3 Results and discussions

3.1 Evaporation-driven SDS crystallisation and the aggregation of SiO_2 nanospheres from DEG/SDS solution and DEG/H_2O/SiO_2 suspension microdroplet

Before studying the microaggregates obtained from the dried composite microdroplets of the DEG/SDS/H_2O/SiO_2 mixture, we first investigated the less complex situation as a basis for farther study, *i.e.* the crystallisation of SDS from DEG/SDS solution and the aggregation of SiO_2 nanospheres in microdroplets of DEG/H_2O/SiO_2 colloidal suspension. These provided the necessary references for further analysis of the mutual influence of the SDS and SiO_2 on the final morphology of the composite microobjects.

Figures 2(a) and (b) present SEM micrographs of the final dry SDS crystallised microobjects obtained by drying microdroplets of DEG/SDS solution. These microproducts are compared to SiO_2 nanosphere aggregates (figs. 2(c) and (d)) obtained from drying microdroplets of the DEG/SiO_2/H_2O colloidal suspension. It can be seen that the microobject shown in fig. 2(a) was rather a flat structure. A probable scenario was that, the SDS crystallised microproduct was mechanically unstable and collapsed inwards under its own weight [48] after the deposition on the substrate. For larger initial droplet diameter but at the same initial concentration of SDS, we obtained a micro apple-like 3D dry SDS microobject (fig. 2(b)). However, the crystallised surface of this SDS microproduct had cracks and pores. These defects can be understood as due to the drying process. We anticipated that SDS crystallised into a porous network of SDS surface films or crystal layers at the droplet surface [18, 20]. This process is understood to be due to charge shielding between the SDS micelles [49]. At a certain stage, the inner core of the SDS crystallised microobject may have contained residues of the solvent. As the drying process proceeded, the solvent then evaporated from inside the structure through the pores visible on the surface. However, it should be noted here that some of the cracks seen on the surface may be artefacts created by the SEM imaging.

For DEG/SiO_2/H_2O colloidal suspension, the final aggregates observed (*e.g.*, fig. 2(c)) were spherical. For initially smaller microdroplets, they had regularly ordered SiO_2 nanospheres at the surface, similar to the earlier ones we reported in [19]. However, aggregates obtained from larger droplets (fig. 2(d)) seemed to exhibit some translational symmetry. This is mostly controlled by the drying rate.

Both SDS microcrystals and SiO_2 nanospheres aggregates show only compact surface inheriting some of the spherical symmetry of the initial droplet.

3.2 Morphologies of composite SDS-SiO_2 microobjects

On the contrary, it can be seen from fig. 3, that drying of composite microdroplets of DEG/SDS solution with H_2O/SiO_2 colloidal suspension for a variety of initial parameters leads to diverse structures exhibiting different kinds of order. The characteristic variation is associated with a differently developed surface. It can be attributed to the mutual influence of SDS and the SiO_2 nanospheres during the drying process. In order to probe this process, we used composite microdroplets of different initial diameters and changed the initial concentrations of SDS. The most essential observation was the stabilising role of SiO_2 nanospheres, serving as the mechanical support for the SDS crystallised surface layers compressed by the effect of surface tension. However, SiO_2 nanospheres themselves show no (or very little) order.

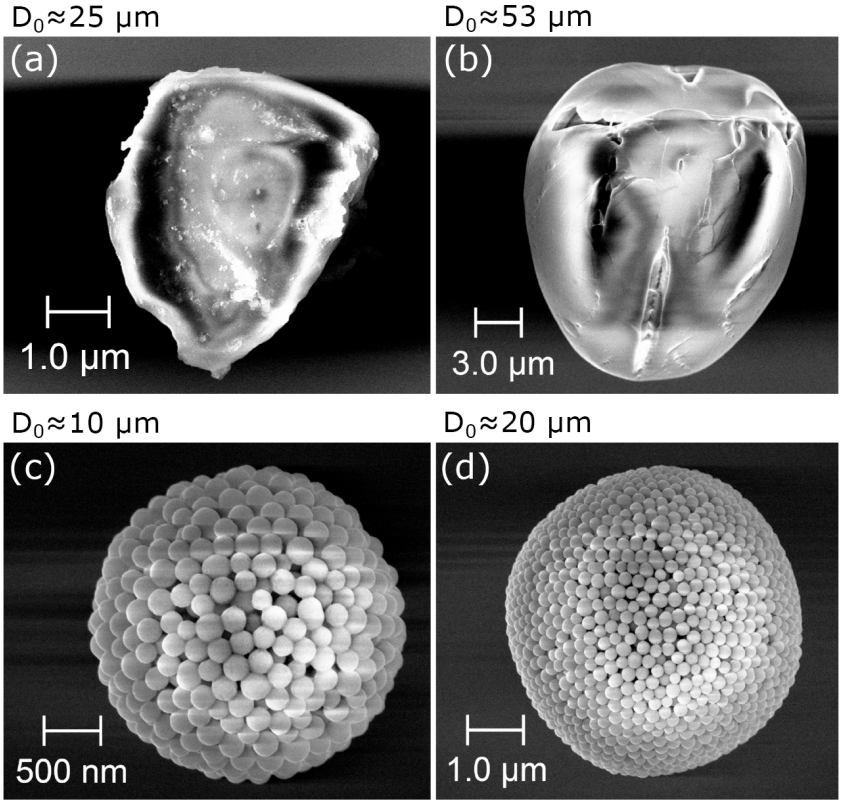

Fig. 2. SEM micrographs of dried microproducts formed by the evaporation of free droplets composed of DEG/SDS solution (a, b) and from DEG/H_2O/SiO_2 colloidal suspension (c, d). The initial mass proportions of the components in the droplets were: DEG : SDS = 37 : 1 and DEG : H_2O : SiO_2 = 61 : 19 : 1. D_0 is the initial microdroplet diameter.

The smallest observed composite microobject (fig. 3(a)) was created from the microdroplet of initial diameter $\sim 10\,\mu$m with 0.8% of initial SDS mass fraction. The drying process led to the formation of stable spherical SDS/SiO_2 composite entirely covered on the surface by SDS crystal shells with interior filled with SiO_2 nanospheres. However, the internal structure of the SDS could not be inferred at this stage. Most probably, the visible surface defects were pores associated with the slow evaporation of the DEG from inside through the surface layer of the SDS. The SDS/SiO_2 composite microobject shown in fig. 3(b) was obtained with twice smaller mass fraction of SDS and from a microdroplet with initial diameter of $\sim 23\,\mu$m. The amount of SDS was apparently too small to cover the entire surface of the aggregated SiO_2 nanospheres. SDS however crystallised in the form of desert-rose–like structures (plates perpendicular to the surface) with SiO_2 in-between the SDS crystal rose flakes. The microobject presented in fig. 3(b) is compared with another one corresponding to the same initial droplet parameters in fig. 4. For the same initial droplet diameters, composition and drying time, similar dry SDS/SiO_2 composite microobjects with nearly similar morphologies and final sizes can be obtained without any structural variations.

From figs. 3(c) and (d), we infer that the final morphology of the SDS/SiO_2 composite microobjects with comparable external sizes were dependent on the initial mass fraction of SDS in the DEG/SDS/SiO_2/H_2O mixture. Counter-intuitively, the surface of the microobject corresponding to the smaller initial mass fraction of SDS (0.8%) (fig. 3(c)) was covered with thick-stranded layers of SDS crystals whiles for higher initial SDS mass fractions (1.3%) (fig. 3(d)), SDS crystallised into structures of desert-rose–like form with open view (walled micro-compartment) to exposed aggregated nanospheres of SiO_2.

Still larger SDS/SiO_2 composite microobjects obtained from larger microdroplets and at higher initial mass fractions of SDS (2.0%) migrated towards cylindrical symmetry. The observed microobjects have the shape of a beetle-like or thin foil bulbs (fig. 3(e)), or even doughnuts (fig. 3(f)). The external SDS crystallised surface served as a micro-container for the randomly aggregated SiO_2 nanospheres. Figure 5 presents a more systematic study of SDS/SiO_2 composite microobjects obtained by drying microdroplets of different initial diameters but at constant initial mass fraction of SDS (1.3%). The smallest SDS/SiO_2 composite microobject (fig. 5(a)) had aggregated SiO_2 layers arranged in-between the SDS crystallised flakes. The SDS flakes were similar to cabbage leaves (curved lobes) growing on the surface towards the centre. With relatively small increase of the initial diameter of the microdroplets, we observed a steady unfolding of the SDS crystallised surface foils (cabbage leaves) into the desert-rose–like structures (figs. 5(b)–(d)).

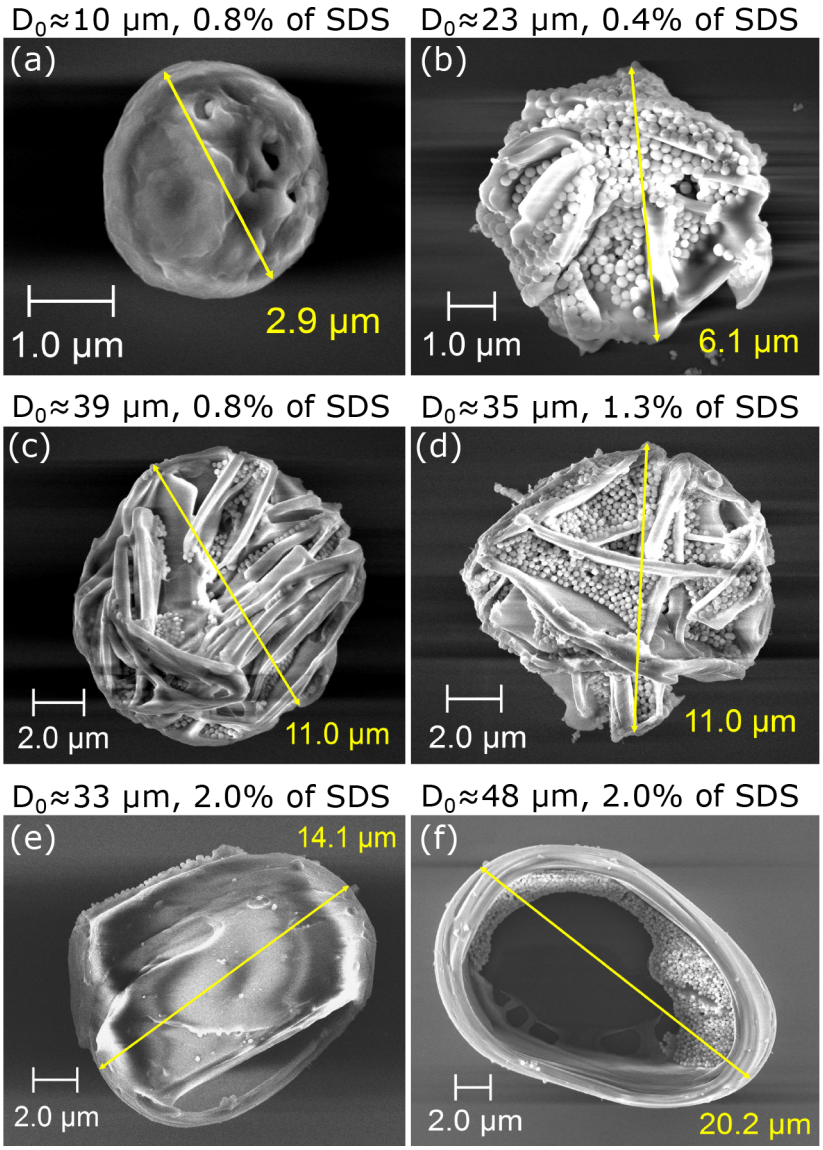

Fig. 3. A representative selection of SEM micrographs of deposited SDS/SiO_2 composite microobjects obtained by drying microdroplets of $DEG/SDS/SiO_2/H_2O$ mixture with different initial SDS mass fractions. The initial mass proportions of the droplet compositions were: (a, c) $DEG : SDS : H_2O : SiO_2 = 96 : 1 : 30 : 2$; (b) $DEG : SDS : H_2O : SiO_2 = 193 : 1 : 60 : 3$; (d) $DEG : SDS : H_2O : SiO_2 = 55 : 1 : 17 : 1$; and (e, f) $DEG : SDS : H_2O : SiO_2 = 74 : 2 : 23 : 1$. D_0 is the initial diameter of the microdroplet.

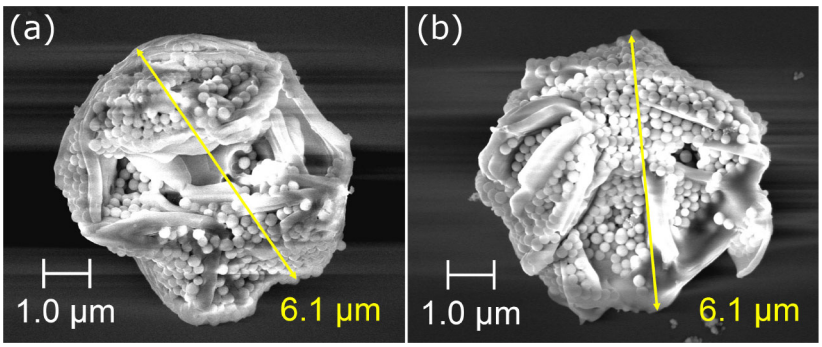

Fig. 4. SDS/SiO_2 composite microobjects obtained by drying composite microdroplets of $DEG/SDS/SiO_2/H_2O$ colloidal suspension with 0.4% mass fraction of SDS. The initial diameters of the droplet in both cases was the same: 23 μm.

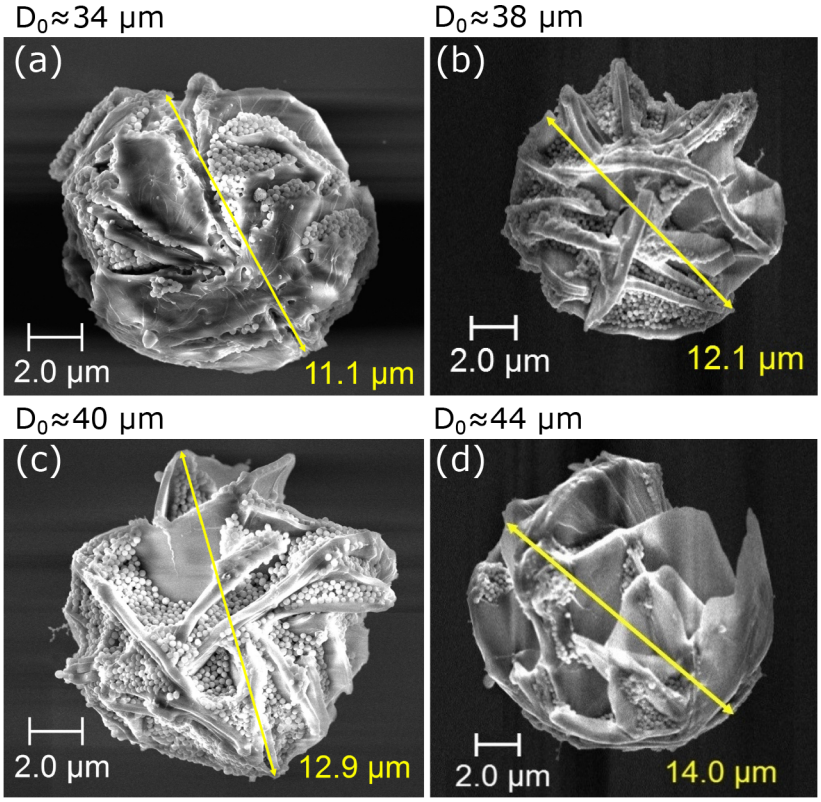

Fig. 5. Variety of SDS/SiO_2 microobjects obtained from drying composite microdroplets of $DEG/SDS/SiO_2/H_2O$ colloidal suspension with constant initial mass fraction of SDS at 1.3%. The final structures are: (a) cabbage-like microobject; (b) desert-rose–like microobject; (c) desert-rose–like microobject; and (d) rose-like microobject. The initial mass proportion of the droplet composition was: $DEG : SDS : H_2O : SiO_2 = 55 : 1 : 17 : 1$. D_0 is the initial diameter of the microdroplet.

Similar trends of the impact of initial droplet size on the SDS/SiO_2 composite structures were also manifested for the higher mass fractions of SDS at 2.0% (fig. 6). Here, the microobjects obtained for increased initial droplet sizes showed an abrupt transition to doughnut-shaped structures with external SDS crystallised surfaces. In fig. 6(a), from an initially smallest microdroplet, we obtained a nearly spherical SDS/SiO_2 composite microobject similar to the one shown in fig. 3(c). However, very few nanospheres of the SiO_2 were visible at the surface of the structure. It appeared that the SiO_2 nanospheres aggregated inside the structure. For the droplets of larger initial diameters, the dry SDS/SiO_2 composite microobjects were doughnut-like structures. The nearly circular structure (fig. 6(b)) changed into deformed ring structures (figs. 6(c), (d)) with respect to increasing initial droplet sizes.

As illustrated in fig. 7 and also in fig. 3 to fig. 6, SiO_2 nanospheres aggregated either inside or outside the SDS crystallised surfaces. It can be expected that the tendency reflects an interplay of coexisting but different interaction forces driving separately the SDS crystallisation process and the aggregation of the SiO_2 nanospheres during the droplet drying process.

3.3 Analysis of surface morphology evolution

In order to comprehend the morphology of the microobjects obtained from our experiments, we review the possible mechanisms leading to the formation of the structures. A microdroplet of colloidal suspension can exhibit complex transitory stages during the process of the evaporation of the dispersant (drying) [50,51]. Initially, the liquid evaporates freely, which is accompanied and driven by heat transport towards the droplet surface [52, 53]. The continuous loss of liquid results in droplet surface recession and increase of SDS and/or the SiO_2 concentration at the droplet surface. Thus, the drying process is increasingly conducted through the interstices between the SiO_2 nanospheres at the surface and the surface layer of SDS. The flow of solution through the interstices between the SiO_2 nanospheres (pores at the surface) can be grasped with the Darcy's law [54, 55] which relates the volume flux J_v [m/s] with the permeability of the medium k [m^2], the fluid viscosity μ [$Pa \cdot s$] and the pressure drop ΔP across the porous material (radius of the droplet R seems to be a good length scale) as

$$J_v = \frac{k}{\mu}\frac{\Delta P}{R}\,. \tag{1}$$

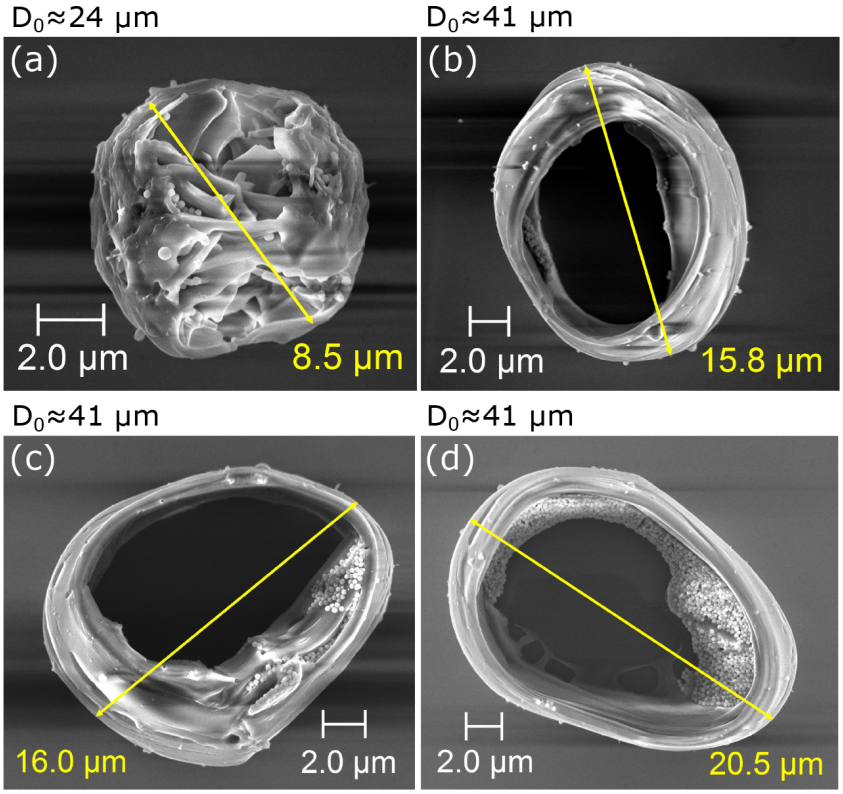

Fig. 6. Variety of SDS/SiO_2 microobjects obtained from drying $DEG/SDS/SiO_2/H_2O$ colloidal suspension with 2.0% of SDS. The external dimensions of the final structures are: (a) spherical shape; (b) nearly circular ring; and (c, d) deformed ring. D_0 is the initial diameter of the microdroplet.

The pressure difference ΔP driving the flow of DEG/SDS solution towards the outer surface is composed of the Laplace pressure due to the curvature of the droplet surface and the capillary pressure p_c due to the porosity of the droplet interior [31,55,56]:

$$\Delta P = \frac{2\gamma}{R} + p_c, \tag{2}$$

where γ is the surface tension of the droplet. The interaction of SiO_2 particles via Van der Waals forces influences both these pressures. Depending on the evolution stage and conditions, the capillary pressure can act either as an opposing or driving force for DEG/SDS solution transport. The interplay of the Laplace and capillary pressures as well as the interaction of SiO_2 nanospheres seemed to have the leading influence on the evolution of morphology of the observed aggregates/microobjects.

Since the Laplace pressure grows with decreasing curvature radius, the transport of the SDS solution from the droplet interior towards the surface is more effective for droplets with smaller radii. In a way, liquid is squeezed by the surface tension from porous interior of the droplet like from a sponge ("sponging effect"). This could explain why smaller observed microaggregates/microobjects are covered with SDS crystals with nearly spherical shapes.

However, for bigger microobjects, spherical symmetry of surface structure is broken and the Darcy's law does not provide a sufficient explanation for their complex shape and the fractionalisation of SiO_2 and SDS (*e.g.*, fig. 7). Differences in interactions between SDS and the SiO_2 nanospheres [38,57] or an interplay of depletion interactions [58, 59] between the two components in the droplet during the drying process with SDS serving as the depletant could be considered.

For even larger droplets at high initial concentration ratio of SDS/SiO_2, the transition from spherical to doughnut-like shapes occurred. We expect that the spherical droplets initially dried isotropically and buckled into final ring structures with SDS crystallised shells supported by the SiO_2 nanospheres. Such transitions can occur when the lateral capillary forces driving the deformation of the droplet surface overcome the electrostatic forces stabilising the suspended particles [6,28,60,61].

In fig. 8 we visualize one of the branches —constant initial mass fraction of SDS at 1.3%— of the evolution of characteristic features of the dried microobjects. A (rough) estimation ($\sim$ 30% accuracy) of fraction of surface coverage by SDS and SiO_2 nanospheres is shown as a function of the dry object final size. Three regions of characteristic

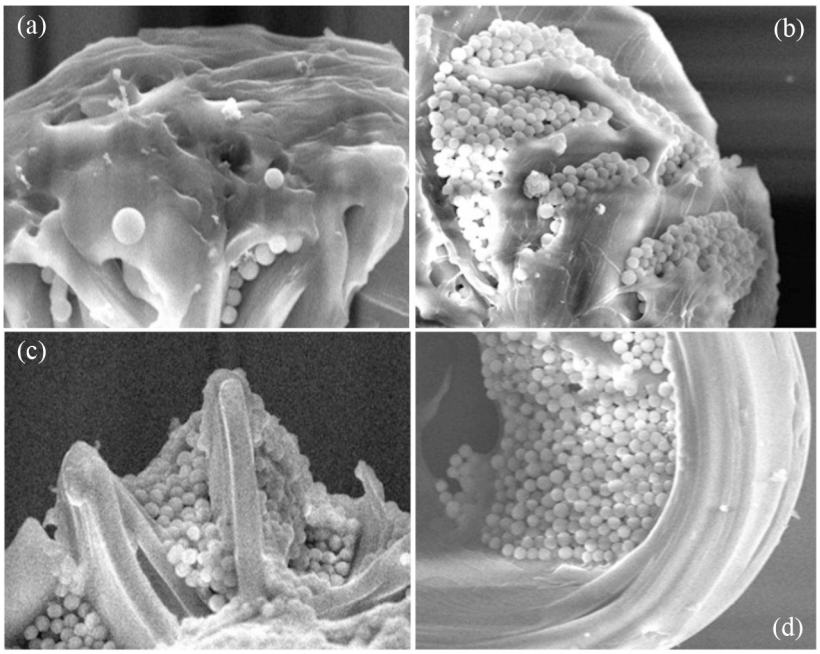

Fig. 7. Landscape of zoomed-in surfaces of SDS/SiO_2 composite microobjects: (a) fully covered with SDS; (b) cabbage-like foils; (c) rose of desert; and (d) doughnut. Silica nanospheres are rather densely but irregularly packed and hardly appear inside crystallised SDS.

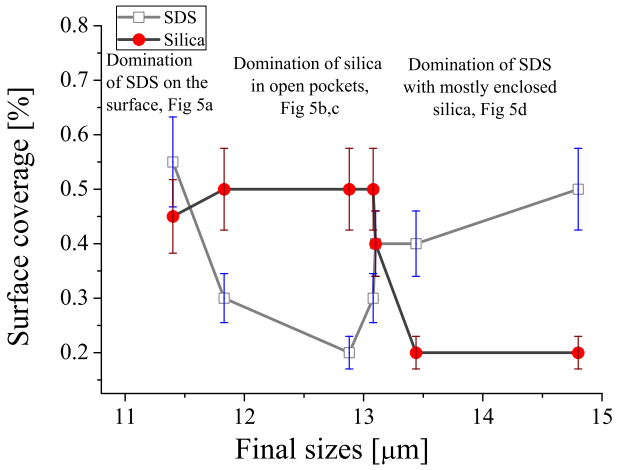

Fig. 8. Evolution of surface coverage fractions of SDS and SiO_2 nanospheres on the dry microobject for the colloidal suspensions (DEG/SDS/SiO_2/H_2O) with 1.3% of SDS. The initial approximate mass fractions of the components of the DEG/SDS/SiO_2/H_2O mixture is DEG : SDS : H_2O : SiO_2 = 61 : 1 : 19 : 1.

features can be identified: i) small objects (below 12 μm) had crystallised surface of SDS foils dominating (fig. 5(a)); ii) transitional structures with partially broken spherical symmetry (12–13 μm) and aggregated SiO_2 nanospheres inside SDS pockets with radially directed sheets of SDS (figs. 5(b), (c)); iii) structures with unfolding of SDS surfaces, and enclosing SiO_2 nanoparticles (above 13 μm, fig. 5(d)).

On the other hand, we analysed the influence of increasing the initial mass fractions of SDS in the DEG/SDS/SiO_2/H_2O mixture for various droplets upon the sizes of the dry microobjects (fig. 9). Statistically, we identified three characteristic size ranges in relation to the final dry microobject symmetry and morphology. The microobjects obtained with final size $\leq 11\,\mu$m had quasi-spherical symmetry (see, *e.g.*, figs. 2(c), (d), 3(a), (c)). Within the range from $\sim 12\,\mu$m to $\sim 15\,\mu$m (figs. 3(d), 3(e) and 5(a)–(c)) various microobjects with partially broken symmetry, ranging from cabbage-like (curved lobes), desert-rose–like structures and thin foil bulb-like structures were obtained. The morphology details of these products were strongly dependent on the initial mass fractions of SDS. For sizes $\geq 15\,\mu$m, doughnut-shaped (figs. 3(f) and 6) structures were obtained.

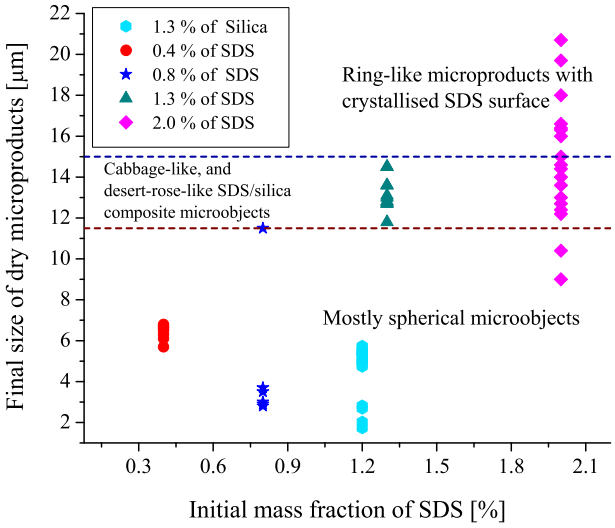

Fig. 9. General statistics of the influence of increasing initial mass fractions (or concentration) of SDS in the DEG/SDS/SiO_2/H_2O mixture for different droplets upon the sizes of the final aggregates/microobjects and their final morphology.

4 Conclusions

We extended the method of drying microdroplets of colloidal suspensions in the LEQT to composite microdroplets of DEG/SDS solution with H_2O/SiO_2 colloidal suspension and demonstrated that structures of diversely developed surface, exhibiting different kinds of order can be produced. The quasi-spherical symmetry imposed by surface tension on a drying droplet is retained at microscale, though at nanoscale (surface structure) it is broken. SiO_2 nanospheres served as a frame for SDS crystalisation.

For small initial diameters of microdroplets of DEG/SDS/SiO_2/H_2O, we observed highly spherical shapes of dry composite microobjects with SDS crystallised surfaces surrounding aggregated SiO_2 nanospheres. Bigger dry composite microobjects of SDS/SiO_2 showed complex morphologies and were dependent on the initial droplet diameters and SDS concentrations. We observed SDS foils as on cabbage and desert-rose–like microstructures with radially directed SDS crystallised sheets. The biggest microobjects for higher initial mass fraction of SDS formed doughnuts with tiny SDS surface sheets and contained randomly aggregated SiO_2 nanospheres. The deformation of the observed doughnuts varied depending on the initial droplet size. This variety of final structures changing profoundly with relatively small change of initial droplet parameters provide very interesting prospects since it corresponds to different physicochemical and optical properties.

The formation of small dry SDS-covered microobjects can be qualitatively grasped by applying the Darcy's law to a porous spherical DEG/SDS/SiO_2 aggregate. The mechanisms of formation of larger microobjects can only be tentatively inferred from other authors' studies. The issues to be resolved are the role of SDS micelles in competition/cooperation in the SiO_2 aggregate formation process, the de-mixing effects of the crystallised SDS surface sheets from the aggregated SiO_2 nanospheres, influence of surface and suspended particles charge interactions and others. We aim to pursue the concept further by exploring the use of different surfactants in mixed composite droplets of colloidal suspensions. Currently, development of numerical models that will aid in further understanding of the inclusion interactions, dynamics of the evaporation processes and other physical mechanisms are under way.

We have presented a rather simple and non-costly method for creating complex micro- and nano-structured materials. The uniqueness of the method consists in quasi-spherical symmetry of the material building blocks. Such an approach can be used for engineering the morphology of spray-dried particles. It also opens prospect to developing rigorous models of interaction mechanisms in aggregating colloidal systems.

The authors acknowledge financial support from the National Science Centre (NCN), Poland, grants numbers 2014/13/D/ST3/01882 and 2017/01/X/ST3/00580 as well as the Ministry of Science and Higher Education, Poland.

References

1. Orlin D. Velev, Abraham M. Lenhoff, Eric W. Kaler, Science **287**, 2240 (2000).
2. Teresa Brugarolas, Fuquan Tu, Daeyeon Lee, Soft Matter **9**, 9046 (2013).
3. Debasis Sen, Jose Savio Melo, Jitendra Bahadur, Subhasish Mazumder, Shovit Bhattacharya, Stanislaus Francis D'Souza, Henrich Frielinghaus, Gunter Goerigk, Rudolf Loidl, Soft Matter **7**, 5423 (2011).
4. Shin-Hyun Kim, Seog-Jin Jeon, Seung-Man Yang, J. Am. Chem. Soc. **130**, 6040 (2008).
5. Álvaro G. Marín, Hanneke Gelderblom, Arturo Susarrey-Arce, Arie van Houselt, Leon Lefferts, Johannes G.E. Gardeniers, Detlef Lohse, Jacco H. Snoeijer, Proc. Natl. Acad. Sci. **109**, 16455 (2012).
6. N. Tsapis, E.R. Dufresne, S.S. Sinha, C.S. Riera, J.W. Hutchinson, L. Mahadevan, D.A. Weitz, Phys. Rev. Lett. **94**, 018302 (2005).
7. Eran Rabani, David R. Reichman, Phillip L. Geissler, Louis E. Brus, Nature **426**, 271 (2003).
8. A.D. Dinsmore, Ming F. Hsu, M.G. Nikolaides, Manuel Marquez, A.R. Bausch, D.A. Weitz, Science **298**, 1006 (2002).
9. Asep Suhendi, Asep Bayu Dani Nandiyanto, Muhammad Miftahul Munir, Takashi Ogi, Leon Gradon, Kikuo Okuyama, Langmuir **29**, 13152 (2013).
10. B. Binks, T. Horozov, *Colloidal Particles at Liquid Interfaces* (Cambridge University Press, 2006).
11. Vinayak Rastogi, Sonia Melle, Oscar G. Calderón, Antonio A. García, Manuel Marquez, Orlin D. Velev, Adv. Mater. **20**, 4263 (2008).
12. Enrico Sowade, Thomas Blaudeck, Reinhard R. Baumann, Cryst. Growth Design **16**, 1017 (2016).
13. Ji-Eun Park, Danielle Reifsnyder Hickey, Sangmi Jun, Seulki Kang, Xiaole Hu, Xi-Jun Chen, So-Jung Park, Adv. Funct. Mater. **26**, 7791 (2016).
14. Jimmy Perdana, Martijn B. Fox, Maarten A.I. Schutyser, Remko M. Boom, Food Bioprocess Technol. **6**, 964 (2013).
15. Alejandro Sosnik, Katia P. Seremeta, Adv. Colloid Interface Sci. **223**, 40 (2015).
16. Asep Bayu Dani Nandiyanto, Kikuo Okuyama, Adv. Powder Technol. **22**, 1 (2011).
17. Vicente João, Pinto João, Menezes José, Gaspar Filipe, Powder Technol. **247**, 1 (2013).
18. F. Moreau, P. Colinet, S. Dorbolo, Phys. Fluids **25**, 091111 (2013).
19. M. Woźniak, G. Derkachov, K. Kolwas, J. Archer, T. Wojciechowski, D. Jakubczyk, M. Kolwas, Langmuir **31**, 7860 (2015).
20. J. Archer, M. Kolwas, D. Jakubczyk, G. Derkachov, M. Woźniak, K. Kolwas, J. Quant. Spectrosc. Radiat. Transf. **202**, 168 (2017).
21. Wolfgang Paul, Rev. Mod. Phys. **62**, 531 (1990).
22. Davis E. James, Schweiger Gustav, *The Airborne Microparticle: Its Physics, Chemistry, Optics, and Transport Phenomena* (Springer, Berlin, Heidelberg, 2002).
23. E. James Davis, A.K. Ray, J. Colloid Interface Sci. **75**, 566 (1980).
24. Robert Hołyst, Marek Litniewski, Daniel Jakubczyk, Marcin Zientara, Mariusz Woźniak, Soft Matter **9**, 7766 (2013).
25. Robert Hołyst, Marek Litniewski, Daniel Jakubczyk, Soft Matter **13**, 5858 (2017).
26. D.S. Lapitskiy, V.S. Filinov, L.V. Deputatova, L.M. Vasilyak, V.I. Vladimirov, V.Ya. Pecherkin, High Temperature **53**, 1 (2015).
27. Geon Dae Moon, Sungwook Ko, Yuho Min, Jie Zeng, Younan Xia, Unyong Jeong, Nano Today **6**, 186 (2011).
28. D. Sen, S. Mazumder, J.S. Melo, Arshad Khan, S. Bhattyacharya, S.F. D'Souza, Langmuir **25**, 6690 (2009).
29. Debasis Sen, Jitendra Bahadur, Shamsuddin Mazumder, Verma G., Puthusserickal A. Hassan, Shovit Bhattacharya, Vijai K., Pankaj Doshi, Soft Matter **8**, 1955 (2012).
30. George Karapetsas, Kirti Chandra Sahu, Omar K. Matar, Langmuir **32**, 6871 (2016).
31. Peter A. Kralchevsky, Nikolai D. Denkov, Curr. Opin. Colloid Interface Sci. **6**, 383 (2001).
32. Joshua R. Trantum, Mark L. Baglia, Zachary E. Eagleton, Raymond L. Mernaugh, Frederick R. Haselton, Lab Chip **14**, 315 (2014).
33. Rong Guo, Liu Tianqing, Yu Weili, Langmuir **15**, 624 (1999).
34. P. Kékicheff, J. Colloid Interface Sci. **131**, 133 (1989).
35. Emil Chibowski, Aleksandra Szczes, Lucyna Holysz, Langmuir **21**, 8114 (2005).
36. Ruhina M. Miller, Andreas S. Poulos, Eric S.J. Robles, Nicholas J. Brooks, Oscar Ces, João T. Cabral, Cryst. Growth Design **16**, 3379 (2016).
37. Yang Zhao, Tao Yu, Xin Tan, Chuang Xie, Shucong Wang, Dalton Trans. **44**, 20475 (2015).
38. Donya Ramimoghadam, Mohd Zobir Bin Hussein, Yun Hin Taufiq-Yap, Int. J. Mol. Sci. **13**, 13275 (2012).
39. Adam J. Blanch, Joe G. Shapter, J. Phys. Chem. B **118**, 6288 (2014).
40. Yu Miao, Haijiao Zhang, Shuai Yuan, Zheng Jiao, Xuedong Zhu, J. Colloid Interface Sci. **462**, 9 (2016).
41. Geetanjali Mishra, Barsha Dash, Ajit Dash, I.N. Bhattacharya, Cryst. Res. Technol. **51**, 433 (2016).
42. Binita Pathak, Saptarshi Basu, J. Appl. Phys. **117**, 244901 (2015).
43. Gröger Henriette, Kind Christian, Leidinger Peter, Roming Marcus, Feldmann Claus, Materials **3**, 4355 (2010).
44. Hartmut Ulmke, Thomas Wriedt, Klaus Bauckhage, Chem. Eng. Technol. **24**, 265 (2001).
45. Daniel C. Taflin, S.H. Zhang, Theresa Allen, E. James Davis, AIChE J. **34**, 1310 (1988).
46. E.J. Davis, M.A. Bridges, J. Aerosol Sci. **25**, 1179 (1994).
47. Sofija Vulgarakis Minov, Frédéric Cointault, Jürgen Vangeyte, Jan G. Pieters, David Nuyttens, Crop Protection **69**, 18 (2015).
48. S. Manley, J.M. Skotheim, L. Mahadevan, D.A. Weitz, Phys. Rev. Lett. **94**, 218302 (2005).

49. Jariya Buajarern, Laura Mitchem, Jonathan P. Reid, J. Phys. Chem. A **111**, 11852 (2007).
50. G. Derkachov, K. Kolwas, D. Jakubczyk, M. Zientara, M. Kolwas, J. Phys. Chem. C **112**, 16919 (2008).
51. M. Mezhericher, A. Levy, I. Borde, Chem. Eng. Sci. **66**, 884 (2011).
52. Hans R. Pruppacher, James D. Klett, *Microphysics of clouds and precipitation* (Kluwer Academic Publishers, Dordrecht, Boston, 1940) 2nd revised and enlarged edition (1997).
53. Sheldon K. Friedlander, *Smoke, Dust, and Haze: Fundamentals of Aerosol Dynamics* (Oxford University Press, New York, 2000) second edition.
54. Stephen Whitaker, Adv. Heat Transf. **13**, 119 (1977).
55. J. Bear, *Dynamics of Fluids in Porous Media* (Dover Publications, 2013).
56. Dan Guo, Guoxin Xie, Jianbin Luo, J. Phys. D **47**, 013001 (2014).
57. N.M. Kovalchuk, V.M. Starov, Adv. Colloid Interface Sci. **179-182**, 99 (2012).
58. Y. Mao, M.E. Cates, H.N.W. Lekkerkerker, Physica A **222**, 10 (1995).
59. Buzzaccaro Stefano, Piazza Roberto, Colombo Jader, Parola Alberto, J. Chem. Phys. **132**, 124902 (2010).
60. D. Sen, J. Bahadur, S. Mazumder, S. Bhattacharya, Soft Matter **8**, 10036 (2012).
61. Hui Xu, Sonia Melle, Konstantin Golemanov, Gerald Fuller, Langmuir **21**, 10016 (2005).